

# Relationship between EUV microflares and small-scale magnetic fields in the quiet Sun

Fayu JIANG, Jun ZHANG, Shuhong YANG

*Key Laboratory of Solar Activity, National Astronomical Observatories,*

*Chinese Academy of Sciences, Beijing 100012, China*

*jiangfayu@nao.cas.cn, zjun@nao.cas.cn, shuhongyang@nao.cas.cn*

(Received ; accepted )

## Abstract

Microflares are small dynamic signatures observed in X-ray and extreme-ultraviolet channels. Because of their impulsive emission enhancements and wide distribution, they are thought to be closely related to coronal heating. By using the high resolution 171 Å images from the Atmospheric Imaging Assembly and the lines-of-sight magnetograms obtained by the Helioseismic and Magnetic Imager on board the *Solar Dynamics Observatory*, we trace 10794 microflares in a quiet region near the disk center with a field of view of  $960'' \times 1068''$  during 24 hr. The microflares have an occurrence rate of  $4.4 \times 10^3 \text{ hr}^{-1}$  extrapolated over the whole Sun. Their average brightness, size, and lifetime are  $1.7 I_0$  (of the quiet Sun),  $9.6 \text{ Mm}^2$ , and 3.6 min, respectively. There exists a mutual positive correlation between the microflares' brightness, area and lifetime. In general, the microflares distribute uniformly across the solar disk, but form network patterns locally, which are similar to and matched with the magnetic network structures. Typical cases show that the microflares prefer to occur in magnetic cancellation regions of network boundaries. We roughly calculate the upper limit of energy flux supplied by the microflares and find that the result is still a factor of  $\sim 15$  below the coronal heating requirement.

**Key words:** Sun: corona — Sun: flares — Sun: magnetic fields

## 1. Introduction

Bright points (BPs) are small-scale, roundish, dynamic structures observed in X-ray and extreme-ultraviolet (EUV) channels and have caused great concerns since their first discovery in rocket X-ray images by Vaiana et al. (1973). Golub et al. (1974) found the BPs had a spatial size of about  $10^8 \text{ km}^2$  and a mean lifetime of 8 hr from the *Skylab* X-ray images. Habbal & Withbroe (1981) observed BPs in EUV channels and found the BPs showed large intensity variations in

a few minutes. The BPs are widespread throughout the whole solar atmosphere, e.g., in the corona (Chandrasekhar et al. 2013), the photosphere (Berger et al. 2007) and the transition region (Harrison 1997). They are observed in active regions (e.g., Shimizu 1995; Berghmans et al. 2001; Romano et al. 2012), coronal holes (Habbal et al. 1990; Doschek et al. 2010; Kamio et al. 2011), and quiet regions (Habbal et al. 1990; Zhang et al. 2001; Kamio et al. 2011). Being observed by different instruments in different wavelengths, they have been given many different names, for example, active-region transient brightenings, blinkers, coronal BPs, microflares, nanoflares, X-ray BPs, X-ray jets, etc. (see Parnell 2002; Aschwanden 2004). Although their physical nature is not fully understood, these small-scale phenomena may share similar physical processes. BPs are found to be associated with dipolar magnetic fields (Golub et al. 1974), and the corresponding total flux surpass that of active regions (Golub & Pasachoff 1997).

The massive energy involved in the BPs, together with their widespread distribution among the solar surface, make small transient events heating mechanism a promising candidate in solving coronal heating problem. The idea of small reconnection events responsible for coronal heating was proposed by Levine (1974), and then developed by Parker (1988) who suggested that the magnetic foot-point motion could form many small current sheets heating the corona via Ohmic dissipation. From balloon-borne observations, Lin et al. (1984) discovered many small hard X-ray microflares with energies between  $10^{24} - 10^{27}$  ergs. Porter et al. (1987) suggested the BPs observed in the EUV line, which lied above the neutral lines of dipoles, were microflares and drivers of spicules. Hudson (1991) pointed out that if the power law index of energies distribution  $\alpha > -2$ , large flares dominated the corona heating, otherwise small flares dominated. Various studies have suggested the power law index lied in  $-2.7 < \alpha < -1.5$  (see Parnell & De Moortel 2012). Statistical study of microflares in active regions by Shimizu (1995) demonstrated these small transient brightenings had an energy range of  $10^{27} - 10^{29}$  ergs and a similar frequency distribution with larger hard X-rays flares. Since the microflaring events in active regions couldn't provide enough energy to heat the solar corona, new studies focused on the small events in the quiet Sun. The microflares in the quiet corona were investigated by Krucker et al. (1997), who found these events have an occurrence rate of one per three seconds extrapolated over the solar surface and the thermal energy of every event is  $10^{25} - 10^{26}$  ergs. Aschwanden et al. (2000) detected 281 flare-like events in the energy range of  $10^{24} - 10^{26}$  ergs in the 171 Å and 195 Å channels with the *Transition Region And Coronal Explorer* (TRACE; Handy et al. 1999) satellite. They found that these small flare-like events were miniature versions of larger flares in soft and hard X-rays and that their energy flux was a factor  $\approx 300$  below the quiet coronal heating requirements. With the *Solar and Heliospheric Observatory* (SOHO; Domingo et al. 1995) observations, Benz & Krucker (2002) estimated that the energy input of EUV microflares was about 10% of the radiative output in the same region. Hannah et al. (2008) analyzed the thermal and non-thermal properties of microflares which had a mean thermal energy of  $10^{28}$  ergs at the time of peak emission in 6 – 12 keV. The characteristics of

microflares in coronal holes and in quiet regions are studied by Kamio et al. (2011) and these microflares were found to share common characteristics to active region flares. With combined the *Solar Dynamics Observatory* (*SDO*; Pesnell et al. 2012) and *Reuven Ramaty High Energy Solar Spectroscopic Imager* (*RHESSI*; Lin et al. 2002) observations, Inglis & Christe (2014) presented that 8 of 10 microflares studied were fitted by a uniform differential emission measure profile.

Since Parker (1988) suggested a nanoflare coronal heating theory, the efforts to search the smallest flare events has never been stopped. However, due to the small energy and the resolving capability of scientific instruments, the search and study of small flare-like events have never been satisfactory. It is necessary to examine the characteristics of microflares more carefully with higher resolution data. The launch of *SDO* provides us a brand new chance to study microflares with more elaborate temporal and spatial resolution. In this paper, we name these small-scale impulsive transient events observed in 171 Å as EUV microflares, and focus on their statistical properties, spatial distribution as well as the relationship with small-scale magnetic fields.

## 2. Observations and data analysis

The Atmospheric Imaging Assembly (AIA; Lemen et al. 2012) on board the *SDO* provides high resolution solar images with a pixel size of  $0''.6$  and a cadence of 12 s, while the Helioseismic and Magnetic Imager (HMI; Scherrer et al. 2012; Schou et al. 2012) provides  $0''.5$  resolution and 45 s cadence line-of-sight magnetograms uninterruptedly. In this study, we adopt AIA 171 Å EUV data and HMI line-of-sight magnetograms on 2010 July 20, when there were no active regions on the solar disk. All the data we used have been applied differential rotation correction.

Firstly we select a quiet region with a field of view (FOV) of  $960'' \times 1068''$  around solar center, and then we visually track the microflares one by one in the region. Finally we investigate the position, lifetime, area, brightness of the microflares respectively and determine the occurrence rate of them in latitudinal direction. Totally 10794 microflares are traced in this work. A microflare is identified as follows: (1) We first employ the EUV movies to find microflare-like events with impulsive enhancements as candidates. (2) We select a square region for each event as carefully as possible to make sure that it can cover the target and doesn't include any pixels belong to another one. Most of the time, a square region works well, considering that the occurring rate of microflares is only  $7.2 \times 10^{-4} \text{ Mm}^{-2} \text{ hr}^{-1}$  (10794 microflares in the FOV within 24 hr). However, there are still a few special cases when two events come too close. Under these circumstances, a square region will include pixels from another event, we refer to an irregular shape, which will be shown in Figure 6. (3) We define an intensity enhancement as the difference of the integrated value in the square at the peak time and that at the time just before the event begins. A microflare event is confirmed if the intensity enhancement exceeds

$3\sigma$ , where  $\sigma$  is the standard deviation of the integrated values in the square of each snapshot in the event process. Once a microflare is confirmed, its lifetime, position, area, and brightness are recorded. The position is determined by the brightest point of a microflare at the peak time. In previous studies, the area was often determined by the pixels exceeding a certain brightness level, which would fail for weak brightenings. Considering the sharp gradients between the microflare and its background, we obtain the area of a microflare by summing up the pixels whose value surpass the mean value in the square at the peak time. To remove the projection effect, the projected area is corrected to the real area by a  $\cos(\alpha)$  factor, where  $\alpha$  corresponds to the heliocentric angle. The brightness is averaged over the area and normalized to that of the quiet Sun ( $I_0$ ), which is defined as the mean value of the whole image.

### 3. Results

We trace 10794 microflares totally in the chosen quiet region. For these microflares, their position, lifetime, area, brightness and the occurrence rate in latitudinal direction are investigated. The relationship between the microflares and the underlying magnetic fields are also studied.

#### 3.1. Statistical results of microflares

The left panel of Figure 1 shows the distribution of all the 10794 microflares over the solar disk. Each point indicates a single microflare, neglecting its size, brightness, etc. There exist microflare-concentrated areas, as well as “void” areas without microflares. As a result, the microflares form visible network patterns on the solar disk. Although they occur unevenly in local regions, on the whole, the microflares still have an uniform distribution on the solar disk. We pick two typical regions with the FOV of  $60'' \times 60''$  (outlined by red windows “1” and “2” in panel (a)). Within 24 hr, only one microflare occurred in window “1” and 78 microflares appeared in window “2”. The occurrence rate of microflares are  $2.12 \times 10^{-5} \text{ Mm}^2 \text{ hr}^{-1}$  and  $1.64 \times 10^{-3} \text{ Mm}^2 \text{ hr}^{-1}$ , respectively. The microflares occupy about 0.05% of the solar surface and their occurrence rate is  $1.72 \times 10^{-2} \text{ Mm}^2 \text{ day}^{-1}$ . The right panel of Figure 1 shows the distribution of microflares along the latitudinal direction. Because the center of the FOV lies in the north of the solar equator on July 20, the area in the south hemisphere is less than that in the northern hemisphere. With 5558 microflares in the southern hemisphere and 5236 in the northern one, we get an occurrence rate of  $2.05 \times 10^{-2} \text{ Mm}^2 \text{ day}^{-1}$  in the southern hemisphere, and  $1.48 \times 10^{-2} \text{ Mm}^2 \text{ day}^{-1}$  in the northern hemisphere. In other words, over the whole Sun, the number of microflares occurred in the southern hemisphere is 720 more than those occurred in the northern hemisphere for every hour.

Figure 2 provides the evolution process of a microflare from appearance to disappearance. The arrows in panels (a) and (b) indicate where the microflare is located. The microflare started at 17:25 UT, then grew up and reached its peak at 17:31 UT. After that, it decayed gradually,

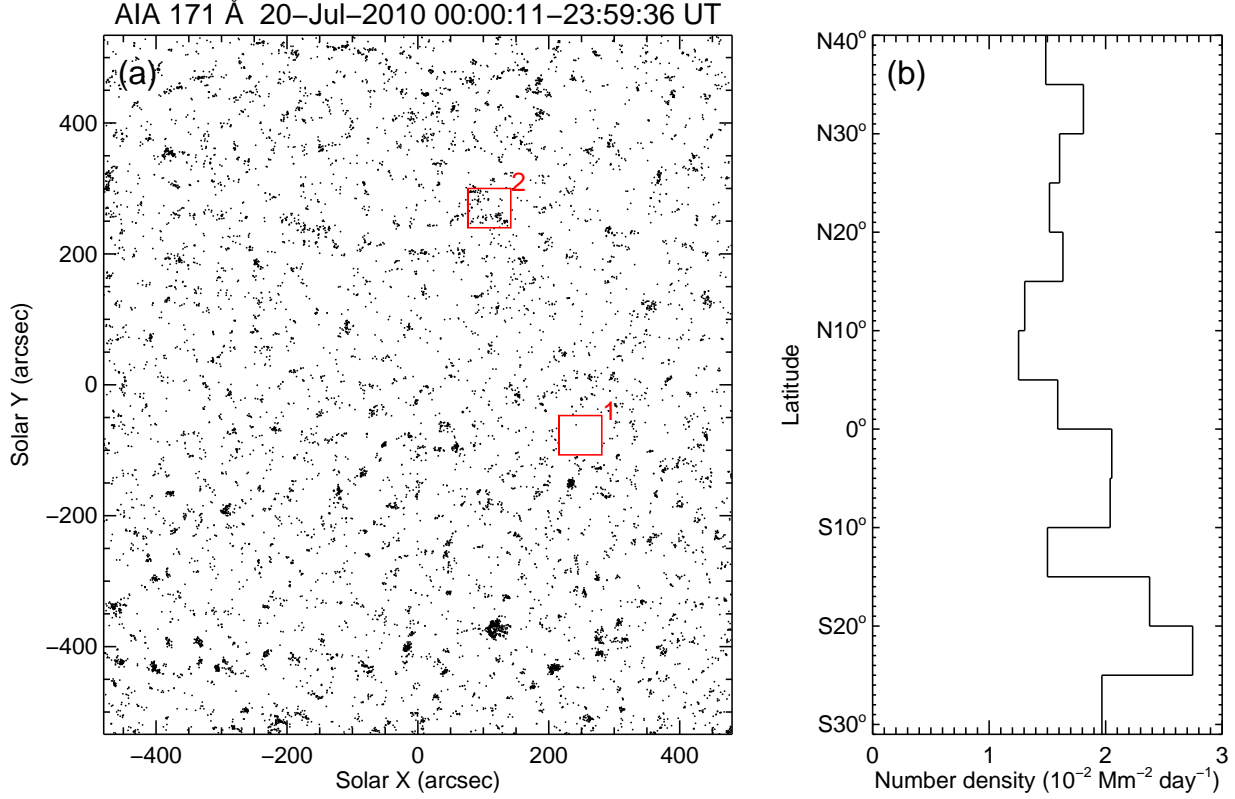


**Fig. 1.** Distribution of the microflares obtained by the *SDO/AIA*. *Panel (a)*: distribution of microflares on the solar disk. Each point indicates a single microflare. Windows “1” and “2” show microflare-scarce and microflare-concentrated regions, respectively. *Panel (b)*: distribution of microflares along the latitudinal direction.

and disappeared finally at 17:37 UT. The brightness, area and lifetime of this microflare are  $7.4 I_0$ ,  $5.2 \text{ Mm}^2$  and 12.0 min, respectively. As can be seen from the three bottom panels, the opposite polarity magnetic fields canceled with each other (outlined by red ellipses). We overlay the microflare on the magnetogram by green contour curve in panel (h) and find that the microflare lies mainly on the cancellation site of opposite polarities. From 17:25 UT to 17:37 UT, the total unsigned magnetic flux decreased by  $2.0 \times 10^{18} \text{ Mx}$  due to the cancellation.

The statistical results of brightness, area, and lifetime, together with their mutual correlation with each other, are shown in Figure 3. The brightness varies from  $0.3 I_0$  to  $5.2 I_0$ . There is a peak located at  $1.5 I_0$ . As the brightness  $I_0$  is obtained by normalizing the full disk, a microflare which takes place in dark background may have a brightness smaller than  $1 I_0$ . As revealed by panel (a2), the area of microflares covers from  $1.2 \text{ Mm}^2$  to  $88.2 \text{ Mm}^2$ , and is most concentrated in the level of  $5.0 \text{ Mm}^2$ . Similar to panels (a1) and (a2), the histogram of lifetime is plotted in panel (a3). The microflares’ lifetime spans from 48 s to 49.2 min, with a peak at 2 min. The mean values of the three parameters are  $1.7 I_0$ ,  $9.6 \text{ Mm}^2$ , and 3.6 min, respectively.

The scatter plots of brightness, area, and lifetime with one another are shown with red

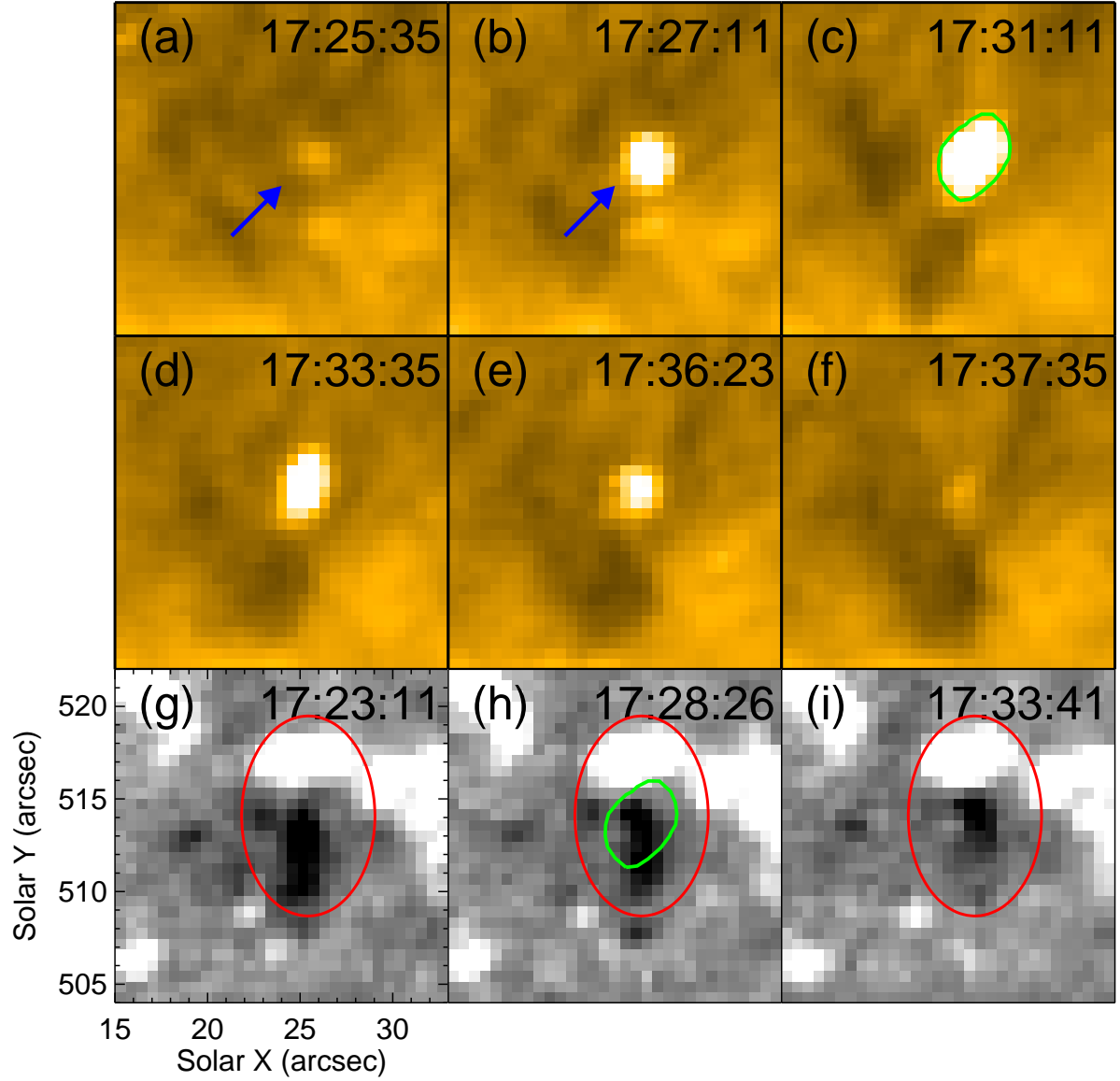


**Fig. 2.** *Panels (a)–(f):* AIA 171 Å images showing the evolution of a microflare. The arrows in panel (a) and panel (b) indicate the location of the microflare. *Panels (g)–(i):* corresponding magnetograms showing the cancellation of opposite polarities, as shown in the red ellipses. The contour of the microflare in panel (c) is overlaid in panel (h) with the green curve.

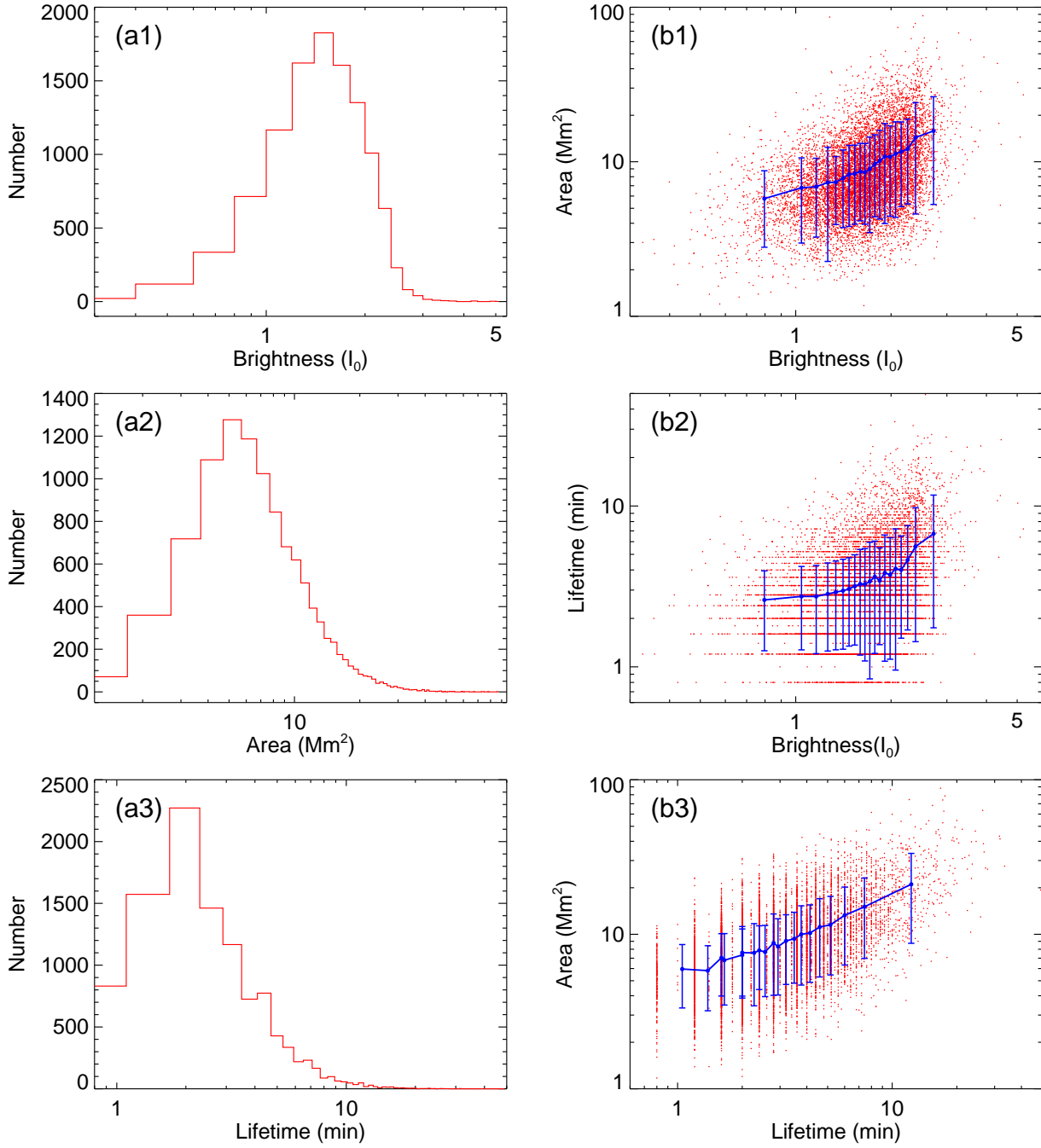


**Fig. 3.** *Panel (a1):* histogram of brightness with a binsize of 0.2  $I_0$ . *Panel (a2):* histogram of area with a binsize of 1.0  $\text{Mm}^2$ . *Panel (a3):* histogram of lifetime with a binsize of 36 s. *Panels (b1), (b2) and (b3):* scatter plots of brightness, lifetime, and area with each other (red symbols) and of sort-grouped points with error bars (blue symbols).



symbols in panels (b1), (b2) and (b3) of Figure 3. The mutual correlations seem quite diffuse. To make the correlations more clear, we apply a “sort-group” method suggested by Zhao et al. (2009). Take panel (b1) for example. Firstly, we sort the area according to the brightness of individuals. Secondly, the sorted data are divided into 19 groups with 540 elements each and one group with 534 elements. Then we get 20 data points by assigning with the mean value of each group. Thirdly, the area and brightness of microflares are correlated with each other and plotted with blue symbols. The error bars are plotted with one standard deviation from the mean value of area in each group in panel (b1). Although the three parameters have large deviations from the mean value in each group, the mutual positive correlation of brightness, area, and lifetime with each other become clear after the trick. The statistical correlations reveal a tendency that the larger microflares have larger brightness and longer lifetimes.

### 3.2. *Relationship between microflares and small-scale magnetic fields*

To study the relationship between the microflares and the small-scale magnetic fields, we randomly select two regions, as shown in Figure 4. The left two panels show all the microflares occurred in the two random picked regions within about 7.5 hr. For each region, every microflare during that period is recorded by a small square window. All the windows in the region are superimposed together to form a new image, as displayed in Figure 4(a) and 4(c). The right two panels display the corresponding magnetic fields, which are obtained by averaging over 30 magnetograms with a cadence of 15 min. We overlay the magnetic contour with  $\pm 15$  G on the microflare images, and mark the microflares’ positions with yellow symbols on the magnetograms. It seems that most of the microflares occur above the network magnetic fields. However, the microflares hardly take place in the uni-polarity network magnetic fields, as indicated by red arrows in panels (c) and (d) of Figure 4. Within the intranetwork area where the magnetic fields are weak, few microflares are seen. These microflares form some network-like patterns, coinciding with the corresponding magnetic network.

We carry out a detail check on the magnetic evolution in two small subregions marked by windows “I” and “II” in panels (c) and (d) of Figure 4. Window “I” is scarce of microflares, with an occurrence rate of  $2.4 \times 10^{-4} \text{ Mm}^{-2} \text{ hr}^{-1}$ , while microflares occur frequently in window “II”, with an occurrence rate of  $4.8 \times 10^{-3} \text{ Mm}^{-2} \text{ hr}^{-1}$ . The evolution sequences of magnetic fields are shown in Figure 5, with window “I” in the top panels and “II” in the bottom panels. To decrease the noise level, three magnetograms with a cadence of 45 s are averaged to form a new one. At 13:29 UT, a magnetic element emerged, which is labeled by arrow “1” in panel (a1). Half an hour later, it had grown larger. Meanwhile, three more turned up, as shown with arrows “2”, “3”, and “4” in panel (a2). At 14:59 UT, these four elements grew larger and separated with each other, which can be seen in panel (a3). In panel (a4), elements “1” and “4” could not be identified anymore. However, elements “2” and “3” still moved further and further. In window “II” where the microflares appear frequently, there are two pair of magnetic



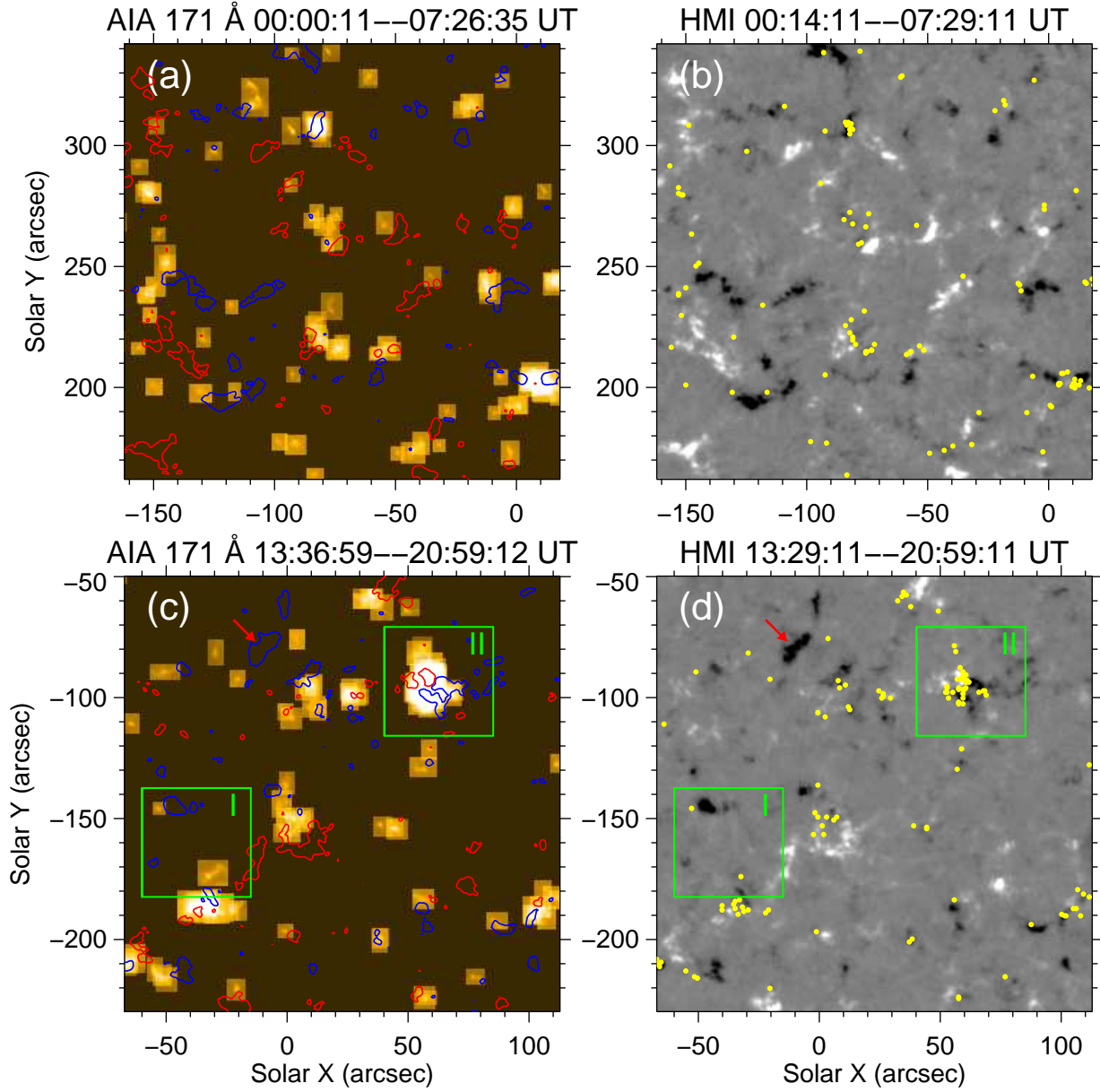


**Fig. 4.** Two random picked regions of microflares and their corresponding magnetic fields. Windows “I” and “II” outline two typical regions. One is scarce of microflares, while the other is prosperous. The red and blue contour lines in the left panels represent  $\pm 15$  G of the magnetic fields, while each yellow point in the right panels stands for a single microflare. The red arrow in panel (d) indicates the uni-polarity network magnetic fields.

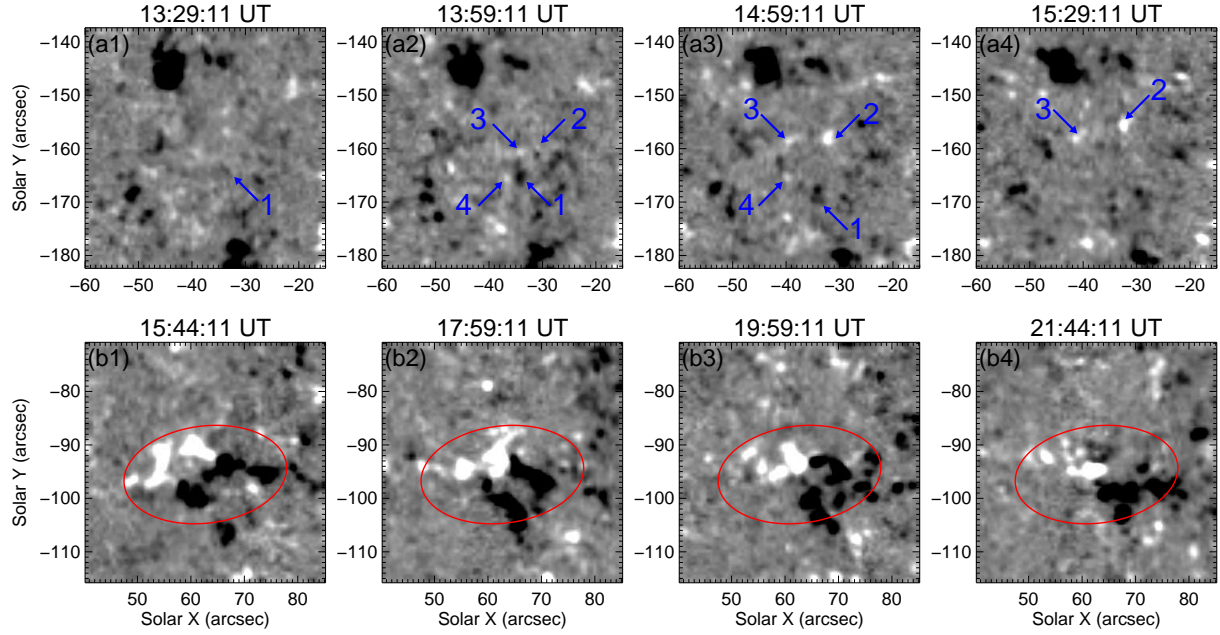


**Fig. 5.** *Panels (a1)–(a4):* sequence of HMI magnetograms outlined by square “I” in Figure 4 (d). Arrows “1”, “2”, “3” and “4” denote four emerging magnetic elements. *Panels (b1)–(b4):* similar to *panels (a1)–(a4)*, but are relevant to the square “II” in Figure 4 (d). The ellipses outline where the magnetic cancellations take place.

elements canceling with each other, as indicated with ellipses in panels (b1) – (b4).

#### 4. Conclusion and discussion

By using the high resolution  $171 \text{ \AA}$  images from AIA and line-of-sight magnetograms obtained by HMI on board the *SDO*, we trace 10794 microflares in a quiet region with a FOV of  $960'' \times 1068''$ . Their statistical properties, spatial distribution and relationship with magnetic fields are investigated. The microflares distribute unevenly in local regions, but on the whole, they have an uniform distribution over the whole region. The occurrence rate is  $1.72 \times 10^{-2} \text{ Mm}^{-2} \text{ day}^{-1}$ , i.e.,  $4.4 \times 10^3 \text{ hr}^{-1}$  extrapolated over the whole Sun. We explore microflares down to 48 s over time scale and to  $1.2 \text{ Mm}^2$  in size. The average size of microflares is  $9.6 \text{ Mm}^2$  and the average lifetime is 3.6 min. By applying a “sort-group” method, we find a mutual positive correlation of the microflares’ brightness, area, and lifetime. The distribution of microflares exhibits network patterns, which are similar to and matched with corresponding magnetic network structures. After a detail check with the magnetograms, we find that the microflares are more concentrated in the magnetic cancellation regions, and hardly take place in the intranetwork regions, where many new small-scale magnetic elements emerge.

Due to the superimposition of microflares in more than 7 hr in the left two panels of Figure 4, it is difficult to resolve individual microflares, especially in the dense regions like the

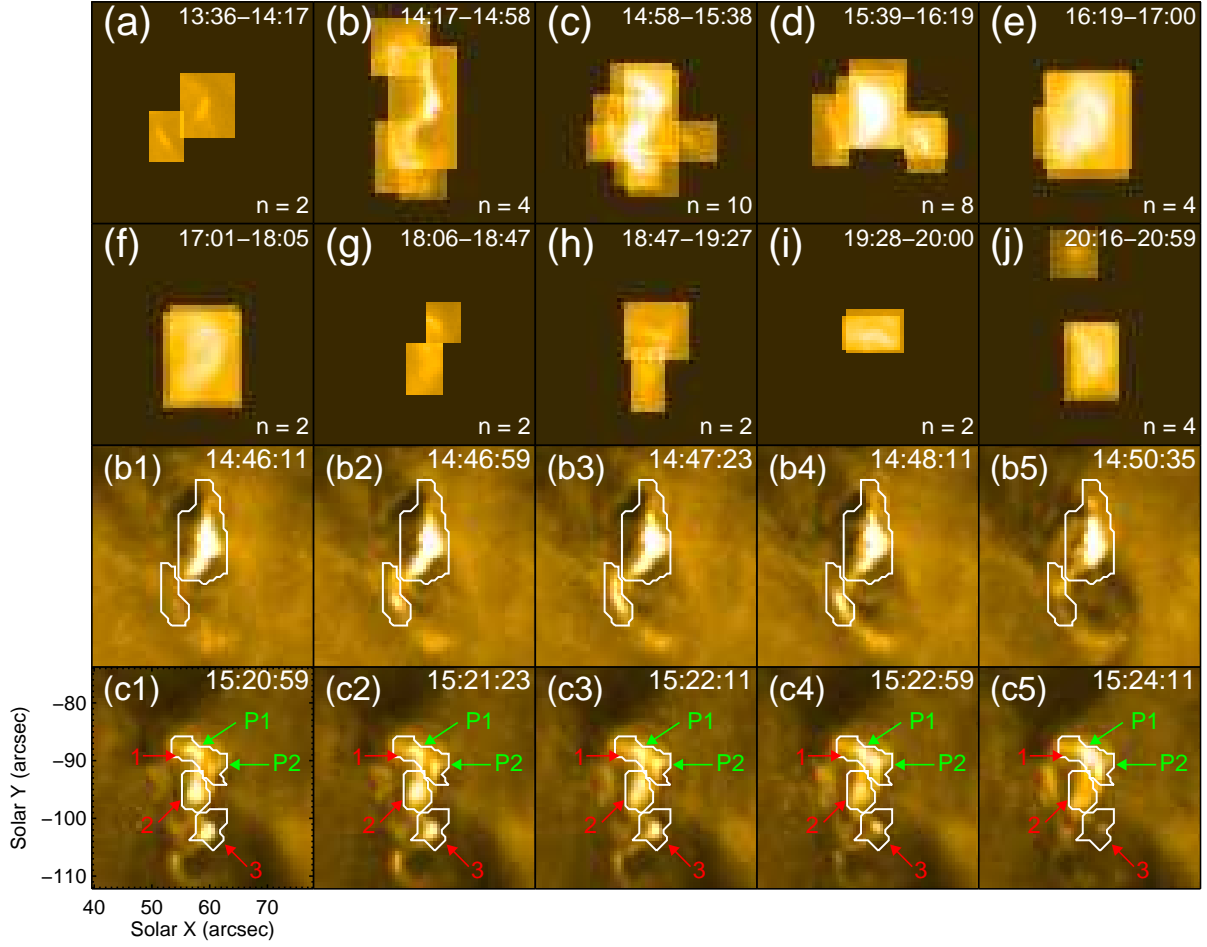


**Fig. 6.** *Panels (a)–(j):* microflares occurred in region “II” of Figure 4 (c), but within about 40 min for each panel. The number of microflares that occurred for each time interval is shown in the lower right corner of each panel. *Panels (b1)–(b5):* sequence of EUV images which demonstrate how to pick up two microflares coming too close in panel (b). *Panels (c1)–(c5):* Arrows “1”, “2”, and “3” denote three microflares recorded in panel (c). Microflare “1” is treated as a single one since “P1” and “P2” merge and can’t be distinguished with each other in their life cycles. The three microflares are tracked similar to those in panels (b1)–(b5).

region “II”. So we dissemble the region “II” in panel (c) of Figure 4 into 10 panels (Figures 6(a)-(j)) with shorter time intervals. The number of microflares occurred for each time interval is given in the bottom-right of each panel. As mentioned in Section 2, the method of picking up microflares with square regions will fail for very special cases. Panels (b1)–(b5) and (c1)–(c5) in Figure 6 show two special examples how we deal with these situations. In panel (b), there were two microflares coming close in space and in time. So we employ an irregular shape instead of a square one to pick up one microflare so as not to include pixels from the other, which is shown in panels (b1)–(b5). The methods of microflare identification and parameter determination are the same to those described in Section 2. As shown in panels (c1)–(c5), two impulsive events “P1” and “P2” arose and merged with each other in their lifetime. As they couldn’t be distinguished and tracked individually, “P1” and “P2” were treated as one microflare and investigated as a whole. Together with microflares “2” and “3”, they are tracked with irregular shapes as mentioned above.

Thanks to the high-resolution data provides by *SDO*, we can distinguish microflares with lifetime as short as 48 s and with area as small as  $1.2 \text{ Mm}^2$ . As a result, we observe 3.7 times microflares observed by Krucker et al. 1997 ( $1200 \text{ hr}^{-1}$ ). Zhang et al. (2001) presented a statistical study of coronal BPs and found the average size of a BP is  $110 \text{ Mm}^2$ . Kamio et al. (2011) identified 7 microflares in quiet regions whose area ranges from  $8.4 \text{ Mm}^2$  to  $22 \text{ Mm}^2$ . In our study, the area of microflares covers from  $1.2 \text{ Mm}^2$  to  $88.2 \text{ Mm}^2$  with a peak at  $5.0 \text{ Mm}^2$ , which is much smaller than that in Zhang et al. (2001), but similar to that in Kamio et al. (2011). The typical lifetime of microflares was found to be 5 – 20 min (Habbal & Withbroe 1981; Habbal et al. 1990; Krucker et al. 1997; Benz & Krucker 2002; Kamio et al. 2011). However, more than 80% of the microflares we observed have a lifetime less than 5 min. The statistical correlations reveal a tendency that the larger microflares have higher brightness and longer lifetimes. However, the mutual positive correlation between brightness, area and lifetime may be not a welcome sign for smallest events detection.

Our results reveal that the microflares are prosperous in the magnetic cancellation regions of network boundaries and wilted in the intranetwork regions. Figure 5 suggests such a scenario: new magnetic elements emerge within the intranetwork region, move apart, and then interact with pre-existing network magnetic fields. The reconnection between newly emerged magnetic fields and pre-existing ones results in the microflares. This scenario is consistent with the converging flux model suggested by Priest et al. (1994), which described how two approaching opposite polarities caused a null point that arose into the corona and formed a BP by magnetic reconnection. The ubiquity of microflares across the solar surface is crucial to the coronal heating. The network patterns exhibited by microflares’ distribution are similar to the magnetic network structures. However, whether the “void” area without microflares is a true microflare-free zone or just a result of detection limitation can not be determined yet. Higher resolution observations are needed to make a more careful examination.

Let's make a rough estimation of the energy flux of EUV microflares in our observations. The occurrence rate is about  $4.4 \times 10^3 \text{ hr}^{-1}$  extrapolated over the whole Sun. Taking the upper limit energy of microflares, i.e.,  $10^{27} \text{ erg}$ , then we get an average energy flux of about  $2.0 \times 10^4 \text{ erg s}^{-1} \text{ cm}^{-2}$ . However, the energy flux required for the coronal heating in the quiet Sun is about  $3 \times 10^5 \text{ erg s}^{-1} \text{ cm}^{-2}$  (Withbroe & Noyes 1977). Our result is still a factor of  $\sim 15$  below the coronal heating requirement. We suggest there may exist a sea of nanoflares (Testa et al. 2013) beneath the detection limit. There are also some studies (Aschwanden et al. 2000; Parnell & Jupp 2000) suggesting that the events with picoflare energies may contribute to the coronal heating because of the insufficient energy of nanoflares. Besides, the Alfvén waves (Alfvén 1947), which can transport magneto-convective energy upwards, have been invoked as another promising mechanism to heat the solar corona (van Ballegoijen et al. 2011). De Pontieu et al. (2007) have observed Alfvén waves with sufficient energy in the chromosphere possibly to heat the solar corona. Ubiquitous Alfvén motions have also been observed in the transition region and in the corona by McIntosh et al. (2011) with the *SDO* satellite, although the generation and dissipation of these waves are still not clear. The ubiquitous rotating network magnetic fields (RNFs) and EUV cyclones in the quiet Sun suggested by Zhang & Liu (2011) may be another effective coronal heating mechanism. The field lines are braided by continuous developments of RNFs and then magnetic reconnection occurs in the braiding fields. Thus the stored energy can be released to heat the corona, while the EUV waves following the cyclones transport energy to other places.

We thank the *SDO*/AIA and HMI teams for providing data. This work is funded by the National Natural Science Foundations of China (11221063, 11203037, 11303050), the CAS Project KJCX2-EW-T07, the National Basic Research Program of China under grant 2011CB811403, and the Strategic Priority Research Program – The Emergence of Cosmological Structures of the Chinese Academy of Sciences (No. XDB09000000).

## References

- Alfvén, H. 1947, *MNRAS*, 107, 211
- Aschwanden, M. J. 2004, *Physics of the Solar Corona. An Introduction* (Chichester: Praxis)
- Aschwanden, M. J., Tarbell, T. D., Nightingale, R. W., et al. 2000, *ApJ*, 535, 1047
- Benz, A. O., & Krucker, S. 2002, *ApJ*, 568, 413
- Berger, T. E., Rouppe van der Voort, L., Löfdahl, M. 2007, *ApJ*, 661, 1272
- Berghmans, D., McKenzie, D., & Clette, F. 2001, *A&A*, 369, 291
- Chandrasekhar, K., Krishna Prasad, S., Banerjee, D., Ravindra, B., & Seaton, D. B. 2013, *Sol. Phys.*, 286, 125
- De Pontieu, B., McIntosh, S. W., Carlsson, M., et al. 2007, *Science*, 318, 1574
- Domingo, V., Fleck, B., & Poland, A. I. 1995, *Sol. Phys.*, 162, 1

- Doschek, G. A., Landi, E., Warren, H. P., & Harra, L. K. 2010, *ApJ*, 710, 1806
- Golub, L., Krieger, A. S., Silk, J. K., Timothy, A. F., & Vaiana, G. S. 1974, *ApJL*, 189, L93
- Golub, L., & Pasachoff, J. M. 1997, *The Solar Corona* (Cambridge: Cambridge Univ. Press)
- Habbal, S. R., & Withbroe, G. L. 1981, *Sol. Phys.*, 69, 77
- Habbal, S. R., Withbroe, G. L., & Dowdy, J. F., Jr. 1990, *ApJ*, 352, 333
- Handy, B. N., Acton, L. W., Kankelborg, C. C., et al. 1999, *Sol. Phys.*, 187, 229
- Hannah, I. G., Christe, S., Krucker, S., et al. 2008, *ApJ*, 677, 704
- Harrison, R. A. 1997, *Sol. Phys.*, 175, 467
- Hudson, H. S. 1991, *Sol. Phys.*, 133, 357
- Inglis, A. R., & Christe, S. 2014, *ApJ*, 789, 116
- Kamio, S., Curdt, W., Teriaca, L., & Innes, D. E. 2011, *A&A*, 529, A21
- Krucker, S., Benz, A. O., Bastian, T. S., & Acton, L. W. 1997, *ApJ*, 488, 499
- Lemen, J. R., Title, A. M., Akin, D. J., et al. 2012, *Sol. Phys.*, 275, 17
- Levine, R. H. 1974, *ApJ*, 190, 457
- Lin, R. P., Schwartz, R. A., Kane, S. R., Pelling, R. M., & Hurley, K. C. 1984, *ApJ*, 283, 421
- Lin, R. P., Dennis, B. R., Hurford, G. J., et al. 2002, *Sol. Phys.*, 210, 3
- McIntosh, S. W., de Pontieu, B., Carlsson, M., et al. 2011, *Nature*, 475, 477
- Parker, E. N. 1988, *ApJ*, 330, 474
- Parnell, C. E., & Jupp, P. E. 2000, *ApJ*, 529, 554
- Parnell, C. E. 2002, *SOLMAG 2002. Proceedings of the Magnetic Coupling of the Solar Atmosphere Euroconference*, 505, 231
- Parnell, C. E., & De Moortel, I. 2012, *Royal Society of London Philosophical Transactions Series A*, 370, 3217
- Pesnell, W. D., Thompson, B. J., & Chamberlin, P. C. 2012, *Sol. Phys.*, 275, 3
- Porter, J. G., Moore, R. L., Reichmann, E. J., Engvold, O., & Harvey, K. L. 1987, *ApJ*, 323, 380
- Priest, E. R., Parnell, C. E., & Martin, S. F. 1994, *ApJ*, 427, 459
- Riethmüller, T. L., Solanki, S. K., Martínez Pillet, V., et al. 2010, *ApJL*, 723, L169
- Romano, P., Berrilli, F., Criscuoli, S., et al. 2012, *Sol. Phys.*, 280, 407
- Scherrer, P. H., Schou, J., Bush, R. I., et al. 2012, *Sol. Phys.*, 275, 207
- Schou, J., Scherrer, P. H., Bush, R. I., et al. 2012, *Sol. Phys.*, 275, 229
- Shimizu, T. 1995, *PASJ*, 47, 251
- Testa, P., De Pontieu, B., Martínez-Sykora, J., et al. 2013, *ApJL*, 770, L1
- Utz, D., Hanslmeier, A., Möstl, C., et al. 2009, *A&A*, 498, 289
- Vaiana, G. S., Davis, J. M., Giacconi, R., et al. 1973, *ApJL*, 185, L47
- van Ballegooijen, A. A., Asgari-Targhi, M., Cranmer, S. R., & DeLuca, E. E. 2011, *ApJ*, 736, 3
- Withbroe, G. L., & Noyes, R. W. 1977, *ARA&A*, 15, 363
- Zakharov, V., Gandorfer, A., Solanki, S. K., Löfdahl, M. 2005, *A&A*, 437, L43
- Zhang, J., Kundu, M. R., & White, S. M. 2001, *Sol. Phys.*, 198, 347
- Zhang, J., & Liu, Y. 2011, *ApJL*, 741, L7
- Zhao, M., Wang, J.-X., Jin, C.-L., & Zhou, G.-P. 2009, *Research in Astronomy and Astrophysics*, 9, 933